



# Politecnico di Bari

Repository Istituzionale dei Prodotti della Ricerca del Politecnico di Bari

## A New Voltage Balancing Technique for a Three-Stage Modular Smart Transformer Interfacing a DC Multibus

This is a post print of the following article

*Original Citation:*

A New Voltage Balancing Technique for a Three-Stage Modular Smart Transformer Interfacing a DC Multibus / Pugliese, Sante; Andresen, Markus; Mastromauro, Rosa Anna; Buticchi, Giampaolo; Stasi, Silvio; Liserre, Marco. - In: IEEE TRANSACTIONS ON POWER ELECTRONICS. - ISSN 0885-8993. - STAMPA. - 34:3(2019), pp. 2829-2840. [10.1109/TPEL.2018.2840961]

*Availability:*

This version is available at <http://hdl.handle.net/11589/140753> since: 2022-06-07

*Published version*

DOI:10.1109/TPEL.2018.2840961

*Terms of use:*

(Article begins on next page)

# A New Voltage Balancing Technique for a Three-Stage Modular Smart Transformer Interfacing a DC Multibus

Sante Pugliese, Markus Andresen, *Member, IEEE*, Rosa A. Mastromauro, *Member, IEEE*, Giampaolo Buticchi, *Senior, IEEE*, S.Stasi, *Member, IEEE*, M. Liserre, *Fellow, IEEE*

**Abstract**—DC Smart Grids represent an alternative to traditional AC power distribution systems. The power conversion stage, interfacing the AC and the DC distribution systems, is the enabling technology to manage multiple DC loads and sources. The three-stage Smart Transformer (ST) is a promising solution, because it includes a DC/DC power conversion stage providing a DC Multibus in output. The modular ST architecture supplies several DC outputs, which allow interfacing a DC Smart Grid with the AC power system. In this paper, the three-stage ST is based on a Cascaded H-Bridge (CHB) converter for the AC/DC power conversion, whereas Dual Active Bridge (DAB) converters are adopted for the DC/DC power conversion stage. The peculiarity is that the DC voltage balancing is performed by the DC/DC power conversion stage instead of the CHB converter. It is advantageous for DC Smart Grids applications where the power sharing among the DC sources and loads is often not balanced. The design of the entire control system is based on the detailed small signal model of the AC/DC and DC/DC power conversion stages of the ST. High dynamic performance of the voltage balancing is fulfilled due to the commonly high switching frequency of the DAB converters.

**Index Terms**— Smart Transformer, DC Smart Grids, CHB Converter, DAB converter, DC voltage control.

## I. INTRODUCTION

DC power distribution systems have gained interest in the last years both in transportation applications and in Smart Grids due to the possibility to increase the efficiency of the system, reducing the number of power conversion stages and avoiding harmonic distortion and reactive power management issues [1-6]. Nevertheless, one of the main obstacles towards the spread of the DC Smart Grids is represented by the difficulty to manage multiple DC connections, interfacing with the main AC power distribution system and ensuring flexible operation. DC Smart Grids supply the loads autonomously in island operation, or the

same loads could be supplied by an active rectifier (AC/DC) connected to the AC power distribution system. The storage systems inside the DC Smart Grid should be charged directly by the DC sources or by the AC power system through the active rectifier [7]. Hence the role of the AC/DC power conversion stage is pivotal.

Looking at the future development of the AC power distribution system, a lot of recent research has been devoted to the power electronics interface, which enables to replace the traditional transformer with a Smart Transformer (ST) [8-13]. The aim of the ST is to provide multiple and flexible connections and to provide advanced control functionalities, which the conventional transformer was not able to provide. It has been demonstrated that modular STs can provide higher reliability and availability than non-modular topologies due to fault tolerance capability and possible reconfiguration in case of faults [14-16].

Among the possible ST topologies, the three-stage ST is based on a first AC/DC power conversion stage connected to the MV distribution system, a second DC/DC power conversion stage, which fulfills galvanic isolation and voltage gain variation, and a last DC/AC power conversion stage for providing the LV output [17-18]. In case of modular topologies, the DC/DC power conversion stage provides multiple and flexible outputs, which can be combined in order to create a DC Multibus [4], [19]. Hence, in this scenario, the first two stages of a three-stage modular ST can represent the enabling technology to interface the DC Smart Grids with the main AC power system.

Analyzing the power converters topologies, the Cascaded H-Bridge (CHB) converter, which consists of several H-Bridges connected in series for each phase, is recognized as a potential candidate for the ST, because of its modularity, scalability and high power quality performance. Focusing on the CHB converter, the DC voltage balancing among the different power cells has represented one of the main research topics in order to avoid overvoltages on the power devices. Numerous DC voltage balance techniques have been developed [20-26]. These techniques have been applied to the ST too, where commonly the AC/DC power conversion stage is in charge of the DC voltage balancing. In particular in [27], [28] and [29] a review of the CHB DC voltage balancing techniques for ST application is presented. Many of these techniques aim to achieve both voltage and power balance [30-31]. Differently, for DC Smart Grids applications, the

This work was supported in part by the European Union/Interreg V-A Germany-Denmark, under PE:Region Project, in part by the European Research Council under the European Union's Seventh Framework Programme (FP/2007-2013)/ERC Grant Agreement n. [616344] - HEART and in part the Ningbo Science & Technology Beauru under Grant 2013A31012 and NSFC under Grant 51650110507.

Corresponding author: Rosa A. Mastromauro, University of Florence, Italy (rosaanna.mastromauro@unifi.it).

modular ST has to guarantee the possibility to operate with power unbalances among the different power conversion cells and maintaining the DC-links voltages balanced. Indeed, considering the DC Smart Grids operation, storages, loads and sources cannot be assumed processing the same power at each DC-link. Instead, the loads are supplied to maintain the reference DC voltage value. Besides, recent research in the ST control, such as the power routing technique [32-33], suggests also to manage different power by the different power conversion cells in order to increase the ST reliability.

In Fig. 1, the first two stages of a three-stage ST are shown where the AC/DC power conversion stage is in charge of the DC voltage balancing. Each power cell of the CHB converter is connected to a Dual Active Bridge (DAB) converter, as shown in Fig. 2, creating a DC Multibus. The DAB converter topology offers many advantages, such as: bidirectional power flow, high step up/down capabilities and Zero Voltage Switching (ZVS), depending on the operating condition. The bidirectional power flow capability makes it an attractive choice when it is needed to control power exchange between energy storage and loads, enabling power flow in both directions. The high step up/down voltage capability provides flexibility to the DC Multibus thanks to the possibility to extend the voltage range and to ensure galvanic isolation avoiding faults propagation. In Fig. 1-2  $V_{DC,i}$  denotes the  $i$ -th output voltage of the CHB converter,  $V_o$  denotes the output voltage of the DAB converters. The DC-links provided in output by the DAB converters can be connected to loads, storage, and DC sources separately or can be connected in parallel on the basis of the DC Smart Grid configuration.

Since loads are commonly not equal, the possibility to balance the DC voltages in the DC/DC power conversion stage instead of the first stage (CHB converter) results advantageous due to the proximity to the DC Smart Grid distribution system. It represents the main goal of the present paper.

In the literature, there are proposed very few examples of DC voltage balancing controls operated by the DAB converters stage in ST. In particular, in [34] the loads are supposed to be balanced and the DC voltage imbalances, caused just by mismatch of the DAB parameters, are compensated using a different PI controller for each DAB converter. For this reason the method does not facilitate the practical implementation.

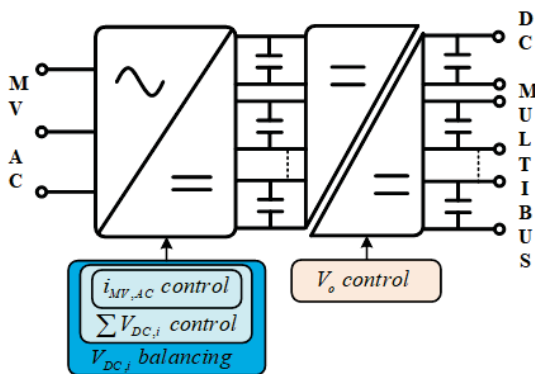


Fig. 1. Control structure of the first and the second stage of a three-stage ST where the AC/DC stage is in charge of the DC voltage balancing function.

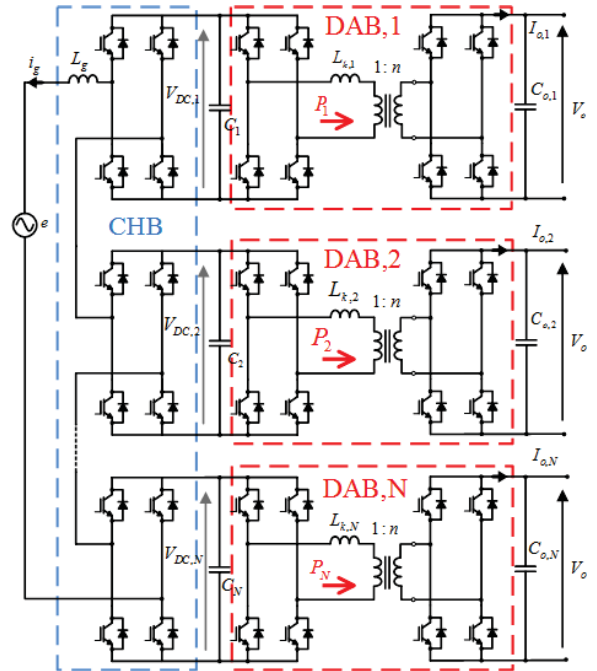


Fig. 2. First and second stage of a three-stage modular ST based on CHB and DAB converters.

A simple and practical control to balance the DC voltages at the output of the DAB converters is proposed in [35] where the phase-shift of each DAB converter is modified differently in order to achieve this purpose. However, no control tuning details are provided in [35] and the dynamics coupling among the DAB converters and the CHB converters is not taken into account. Hence the effect of possible DC-links voltage variations of the CHB converter on the output voltage of the DAB converters are not considered in the control design.

In this work, the small signal modeling of the entire power stage leads to take into account the coupling among the CHB converter and the DAB converters dynamics. The design of the complete control system is based on the detailed small signal model of the AC/DC and DC/DC power conversion stages of the ST. The detailed model of the ST represents one of the main contributions of this work. Very few papers can be found on this topics and in these papers the analysis is focused just on single parts of the ST [36-39].

The proposed control structure of the overall system is represented in Fig. 3. The CHB converter controls the AC current and the CHB DC-links voltages, whereas the DAB converters control their DC-links output voltages, compensating the effects of voltage variations on the DAB converters output. Instability issues are avoided, because all controllers are tuned on the basis of the theoretical model of the ST and high dynamic performances can be achieved. The results are compared with the performances provided in case the DC voltage balancing is performed by the CHB converter.

The DAB converters are characterized by higher switching frequencies than the CHB converter due to the presence of a medium frequency transformer. In case of the CHB converter, such switching frequencies cannot be used in order to achieve an acceptable efficiency [40]. This peculiarity is exploited in order to improve the dynamic performance of the proposed voltage balancing control.

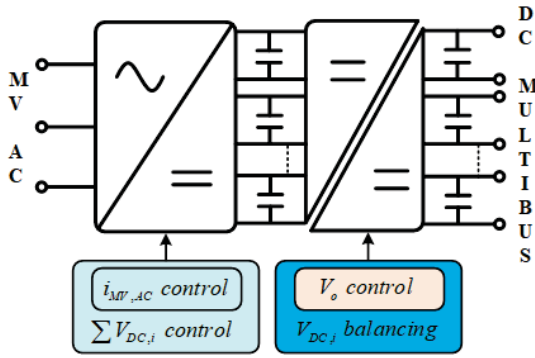


Fig. 3. ST control structure where the DC/DC stage is in charge of DC voltage balancing.

It represents a significant improvement since larger control bandwidth involves plug and play feature to the overall system which can be able to identify and rapidly respond to changes due to DC sources insertion or disconnections, loads variations, etc.

The rest of the paper is organized as follows. In Section II the small signal model of the first and second stage of the ST is presented, in Section III the proposed control scheme is described. The simulation and experimental results are discussed in Section IV. Finally, the conclusion is given in Section V.

## II. MODEL OF THE SMART TRANSFORMER

The considered case-study is shown in Fig. 2. An average model of the ST is shown in Fig. 4. In this model, the CHB converter is represented as the sum of  $N$  voltage sources connected to the main AC grid voltage  $e$  through an inductive filter  $L_g$ .

The output voltage  $v_{AB,i}$  of each CHB power cell can be defined as:

$$v_{AB,i} = m_i V_{DC,i} \quad \text{with} \quad i = 1, 2, \dots, N \quad (1)$$

where  $V_{DC,i}$  is the corresponding DC-link voltage and  $m_i$  the corresponding modulating signal.

The DC current of the  $i$ -th CHB power cell is indicated as  $i_{DC,i}$  and it can be defined as:

$$i_{DC,i} = m_i i_g \quad \text{with} \quad i = 1, 2, \dots, N \quad (2)$$

The DAB converters are represented both in input and in output as current sources, denoting the input current as  $I_{DAB,i}$  and the output current as  $I_{o,i}$ .

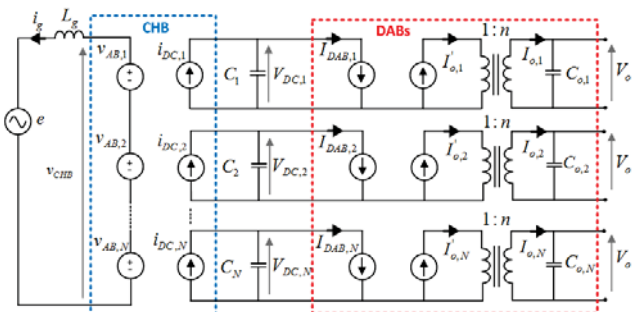


Fig. 4. CHB and DAB converters average model.

The DAB converter average model can be analytically derived studying the behavior of the current that flows through the transformer leakage inductance  $L_k$ . The input and output average currents can be evaluated, as described in [41]. Due to the symmetry of the circuit, the output and input currents over half a cycle of each DAB converter are described with the following equations:

$$I_{DAB,i} = \frac{V_o T_{DAB} \varphi_i (1 - \varphi_i)}{2L_{k,i} n} \quad \text{with} \quad i = 1, 2, \dots, N \quad (3)$$

$$I_{o,i} = \frac{V_{DC,i} T_{DAB} \varphi_i (1 - \varphi_i)}{2L_{k,i} n} \quad \text{with} \quad i = 1, 2, \dots, N \quad (4)$$

where  $n$  is the DAB transformer turn ratio,  $T_{DAB}$  represents the DAB switching period,  $\varphi$  ( $-0.5 < \varphi < 0.5$ ) is the phase-shift angle (expressed in p.u. with respect to  $\pi$ ) between the voltage at the primary and secondary side of the DAB transformer,  $V_o$  is the DAB output voltage.

### A. Model of the CHB converter

Starting from the average model of the CHB converter defined in (1-2), the following equations can be derived describing the CHB converter with unitary power factor operation:

$$L_g \frac{dI_g(t)}{dt} = \sum_{i=1}^N (M_i(t) V_{DC,i}(t)) - E(t) \quad (5)$$

$$C_i \frac{dV_{DC,i}(t)}{dt} = \frac{1}{2} M_i(t) I_g(t) - I_{DAB,i}(t) \quad i = 1, \dots, N \quad (6)$$

where  $E$  is the amplitude of the grid voltage vector,  $I_g$  is the amplitude of the grid current vector and  $M$  is the amplitude of the modulating signal vector. With a perfectly balanced load, therefore with similar voltages, each cell is driven with the same modulating signal:

$$L_g \frac{dI_g(t)}{dt} = N (M(t) V_{DC,i}(t)) - E(t) \quad (7)$$

$$C_i \frac{dV_{DC,i}(t)}{dt} = \frac{1}{2} M(t) I_g(t) - I_{DAB,i}(t) \quad i = 1, \dots, N \quad (8)$$

In (7)-(8), the terms  $M(t) V_{DC,i}(t)$  and  $M(t) I_g(t)$  are nonlinear. The small signal linearization around the equilibrium point at the rated conditions is necessary in order to derive a linear model of the CHB in the Laplace domain.

Neglecting the second-order signal perturbations, the small signal linearization of (7) and (8) leads to:

$$L_g \frac{d\tilde{I}_g}{dt} = N (\tilde{M} \bar{V}_{DC,i} + \bar{M} \tilde{V}_{DC,i}) \quad (9)$$

$$2C_i \frac{d\tilde{V}_{DC,i}}{dt} = \tilde{M} \bar{I}_g + \bar{M} \tilde{I}_g - 2\tilde{I}_{DAB,i} \quad (10)$$

where  $(\tilde{\phantom{x}})$  denotes small perturbation, and  $(\bar{\phantom{x}})$  denotes steady-state value. These two linear equations can be expressed in the Laplace domain, resulting in:

$$\tilde{I}_g(s) = \frac{N\bar{V}_{DC,i}\tilde{M}(s) + N\bar{M}\tilde{V}_{DC,i}(s)}{L_g s} \quad (11)$$

$$\tilde{V}_{DC,i}(s) = \frac{\tilde{M}(s)\bar{I}_g + \bar{M}\tilde{I}_g(s) - 2\tilde{I}_{DAB,i}(s)}{2C_i s} \quad (12)$$

From (11), the small signal modulation signal  $\tilde{M}$  is derived:

$$\tilde{M}(s) = \frac{L_g \tilde{I}_g(s) - N\bar{M}\tilde{V}_{DC,i}(s)}{N\bar{V}_{DC,i}} \quad (13)$$

By substituting (13) in (12), the transfer function between each DC-link voltage and the correspondent AC current and input current of the DAB results in:

$$\tilde{V}_{DC,i}(s) = \frac{\bar{V}_{DC,i}(T_z s + 1)}{\bar{I}_g(T_p s + 1)} \tilde{I}_g(s) - \frac{2\bar{V}_{DC,i}}{\bar{I}_g \bar{M}(T_p s + 1)} \tilde{I}_{DAB,i}(s) \quad (14)$$

where  $T_z$  and  $T_p$  are defined as follows:

$$T_z = \frac{\bar{I}_g L_g}{N\bar{V}_{DC,i} \bar{M}} \quad T_p = \frac{2\bar{V}_{DC,i} C_i}{\bar{I}_g \bar{M}} \quad (15)$$

(14) indicates that the voltage variation on the DC-link of each H-Bridges depends both on the grid current  $\tilde{I}_g$  and DC current  $\tilde{I}_{DAB,i}$  variations. In the model,  $\tilde{I}_{DAB,i}$  is considered as a disturbance to be rejected by the voltage control loop. The small signal model of the CHB converter is depicted in Fig. 5.

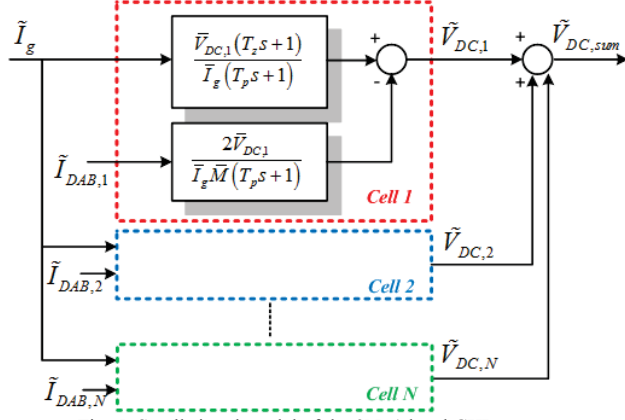


Fig. 5. Small signal model of the 2N+1 level CHB converter.

### B. Model of the DAB converters

The average model of the DAB, as presented in (3)-(4), contains nonlinearity in the actuating term  $\varphi_i(1-\varphi_i)$ . Furthermore, this term is multiplied in (3) with the controlled output voltage  $V_o$  and in (4) it is multiplied with the input voltage  $V_{DC,i}$ .

In order to control the output voltage with a linear controller, it becomes necessary to derive a linear model of the DAB converter around a stable steady-state point. Considering (3)-(4) and a perturbation around their steady-state points, it results:

$$\tilde{I}_{DAB,i} = \frac{T_{DAB}}{2L_{k,i}n} \left[ \tilde{\varphi}_i(1-2\bar{\Phi}_i)\bar{V}_o + \tilde{V}_o(1-\bar{\Phi}_i)\bar{\Phi}_i \right] \quad (16)$$

$$\tilde{I}_{o,i} = \frac{T_{DAB}}{2L_{k,i}n} \left[ \tilde{\varphi}_i(1-2\bar{\Phi}_i)\bar{V}_{DC,i} + \tilde{V}_{DC,i}(1-\bar{\Phi}_i)\bar{\Phi}_i \right] \quad (17)$$

It is assumed that all the DAB converters have the same parameters. For the modeling, all the DAB converters are assumed to provide the same output voltage  $V_o$ , which is DC voltage level chosen for the power distribution system in the Smart Grid. Considering that some of the outputs of the DC Multibus can be connected in parallel on the basis of the configuration of the DC Smart Grid, the small signal model of the overall DC/DC power conversion stage is derived assuming that the DAB converters outputs are parallel connected and supply a resistive load denoted as  $R_o$ :

$$\tilde{I}_o = \sum_{i=1}^N \tilde{I}_{o,i} \quad \tilde{V}_o(s) = \frac{R_o}{(R_o C_o s + 1)} \tilde{I}_o \quad (18)$$

Hence, substituting (17) in (18), it results in:

$$\tilde{V}_o(s) = \frac{R_o}{(R_o C_o s + 1)} \sum_{i=1}^N \left\{ \frac{T_{DAB}}{2L_{k,i}n} \left[ \tilde{\varphi}_i(1-2\bar{\Phi}_i)\bar{V}_{DC,i} + \tilde{V}_{DC,i}(1-\bar{\Phi}_i)\bar{\Phi}_i \right] \right\} \quad (19)$$

It is possible to define two constant gains as:

$$G_{\varphi,i} = \frac{T_{DAB}}{2L_{k,i}n} (1-2\bar{\Phi}_i)\bar{V}_{DC,i} \quad (20)$$

$$G_{V,i} = \frac{T_{DAB}}{2L_{k,i}n} (1-\bar{\Phi}_i)\bar{\Phi}_i$$

Hence the final expression of the output voltage loop is:

$$\tilde{V}_o(s) = \left( \frac{R_o}{R_o C_o s + 1} \right) \sum_{i=1}^N \left[ G_{\varphi,i} \tilde{\varphi}_i + G_{V,i} \tilde{V}_{DC,i} \right] \quad (21)$$

In such control system,  $\tilde{V}_o$  is the controlled variable,  $\tilde{\varphi}_i$  is the input,  $\tilde{V}_{DC,i}$  is considered as an external disturbance and  $R_o C_o$  is the plant time constant. The small signal model of the DC/DC power conversion stage is represented in Fig. 6.

### III. PROPOSED CONTROL SYSTEM

With regard to the case study represented in Fig. 2 and to the control features shown in Fig. 3, the overall control system of the first two stages of the ST can be designed as proposed in the following.

#### A. CHB converter control system

The basic control functions of the CHB converter are the DC voltage control and the AC current control. The outer DC voltage control loop provides the reference to an internal current control loop as shown in Fig. 7. Details about the CHB converter modulation can be found in [4]. Processing a single-phase sinusoidal current, the P+Resonant (PR) controller is a good choice for the inner current loop as already demonstrated in [42].

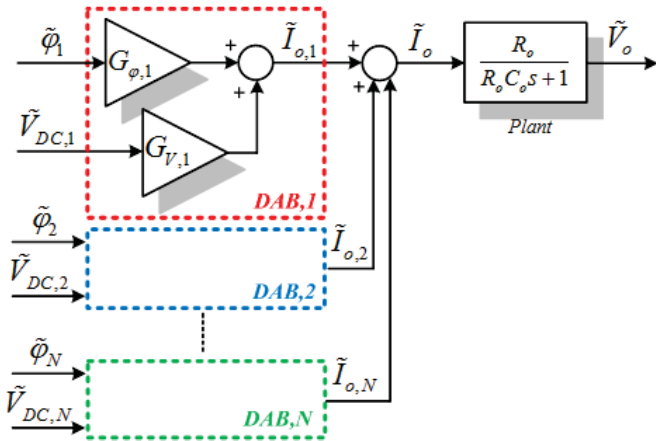


Fig. 6. Small signal model of the DC/DC power conversion stage.

The proportional and resonant gain of the PR controller can be tuned to achieve optimal damping (damping factor  $\zeta=0.707$ ) and short settling times corresponding to an overshoot around 5% in the step response [43]. In this hypothesis a second-order transfer function can be used as a good approximation of the current loop transfer function based on a PR controller:

$$H_{I_g}(s) = \frac{I_g}{I_g^*} \approx \frac{2}{s^2 + \frac{2}{3T_s}s + \frac{2}{(3T_s)^2}} \quad (22)$$

The outer loop is based on a PI controller and the parameters of the PI voltage controller can be tuned in order to decouple the internal current loop and the external voltage loop dynamics. The open loop transfer function of the overall DC voltage control loop is:

$$G_{V_{DC}}(s) = \frac{K_p (T_i s + 1)}{T_i s} H_{I_g}(s) \left( \frac{N \bar{V}_{DC,i} (T_z s + 1)}{\bar{I}_g (T_p s + 1)} \right) \quad (23)$$

where  $K_p$  is the proportional gain,  $T_i$  is the integral time

constant. The design of the voltage control loop is made in order to obtain a dynamics which is ten times slower than the closed loop current dynamics at least.

As first step, the PI integrator time constant  $T_i$  has been chosen equal to the plant time constant  $T_p$ . Considering a perfect pole-zero cancellation, the voltage open-loop transfer function in the Laplace domain is:

$$G_{V_{DC}}(s) = \left( \frac{K_p \bar{M} N}{2C_i} \right) \frac{(T_z s + 1)}{s} H_{I_g}(s) \quad (24)$$

If the current control loop is adjusted to be optimally damped, a first-order approximation can be useful when calculating the bandwidth of the system and when designing the voltage loop with a bandwidth smaller than the one of the current loop [43]:

$$H_{I_g}(s) \approx \frac{1}{(3T_s s + 1)} \quad f_{BW-CC} = \frac{1}{6\pi T_s} \quad (25)$$

Substituting the first-order current loop approximation of (25) in (24), a new simplified open-loop transfer function is derived:

$$G_{V_{DC}}(s) = \frac{k(T_z s + 1)}{s(3T_s s + 1)} \quad \text{with } k = \frac{K_p \bar{M} N}{2C_i} \quad (26)$$

Starting from (26), the closed-loop transfer function of the voltage controller is:

$$H_{V_{DC}}(s) = \frac{k(T_z s + 1)}{3T_s s^2 + (k T_z + 1)s + k} \quad (27)$$

This equation shows the dependence of the closed loop transfer function on the value of  $K_p$ , which is the only tunable parameter to guarantee the bandwidth specifications.

The entire cascaded control system based on the small signal model of the CHB converter is represented in Fig.7.

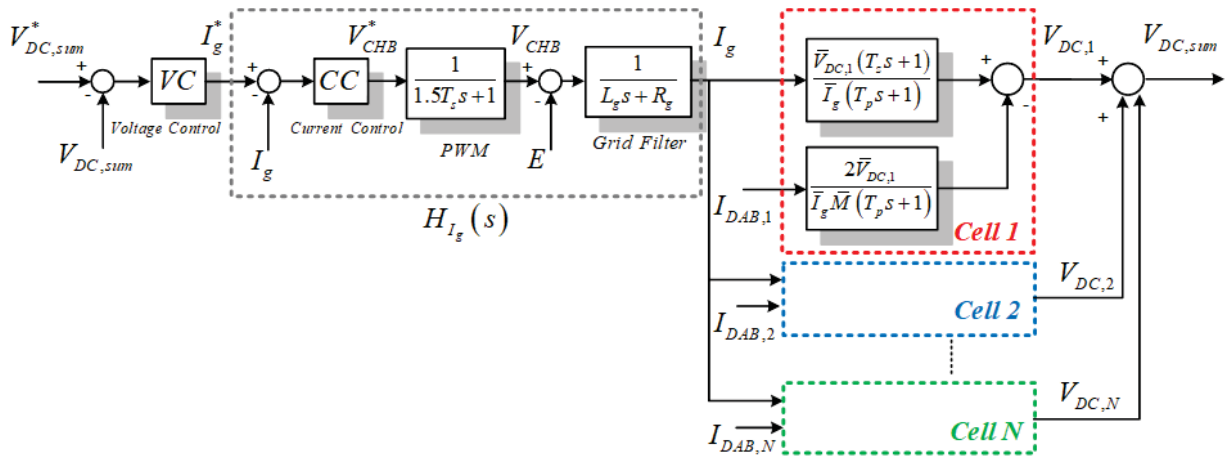


Fig.7. Control scheme of the CHB converter

### B. DAB converters control system

The main task of the DAB converters control system is the regulation of the common output voltage  $V_o$  to its reference value. The control scheme of the DAB converter is shown in Fig. 8. Starting from the equation of the DAB converters output voltage:

$$\tilde{V}_o(s) = \left( \frac{R_o}{R_o C_o s + 1} \right) \left( NG_\varphi \tilde{\varphi} + G_V \sum_{i=1}^N \tilde{V}_{DC,i} \right) \quad (28)$$

a control law can be defined, which considers  $\varphi$  as the control variable and  $V_{DC,i}$  as a measurable disturbance. The effect of the input voltage variations  $\tilde{V}_{DC,i}$  of the DAB converters on the output voltage  $V_o$  can be compensated introducing a feed-forward action whose effect is added up with the feedback control. Just in this hypothesis, the DAB converters control can be decoupled by what occurs in the CHB converter. Hence, the control law results in:

$$\tilde{\varphi} = K_{p_o} \left( 1 + \frac{1}{T_{i_o} s} \right) \left( \tilde{V}_o^* - \tilde{V}_o \right) - \frac{G_V}{NG_\varphi} \sum_{i=1}^N \tilde{V}_{DC,i} \quad (29)$$

The final open loop transfer function is the following:

$$G_{V_o}(s) = NG_\varphi K_{p_o} \left( \frac{T_{i_o} s + 1}{T_{i_o} s} \right) \left( \frac{R_o}{R_o C_o s + 1} \right) \quad (30)$$

where  $K_{p_o}$  and  $T_{i_o}$  are respectively the proportional gain and the integral time constant. Choosing  $T_{i_o}$  equal to  $R_o C_o$  (pole-zero cancellation), the closed loop transfer function  $H_{V_o}(s)$  is derived:

$$H_{V_o}(s) = \frac{1}{\left( 1 + \frac{s}{K_{DAB} K_{p_o}} \right)} \quad \text{with } K_{DAB} = \frac{NG_\varphi}{C_o} \quad (31)$$

It results in a first order system, with reference tracking and disturbance rejection capability depending on the value of the proportional gain.

### C. DC voltage balancing control

The voltage balancing control is based on a PI controller for each DC-link. The phase shift angle for each DAB converter is corrected by subtracting the contribution of the voltage balancing controller  $\Delta\varphi_i$ . This is shown in Fig. 8. Hence, in case of a ST with  $N$  power cells, the phase shift for each DAB converter can be calculated as:

$$\tilde{\varphi}_i = \varphi - K_{pBAL,i} \left( 1 + \frac{1}{T_{BAL,i} s} \right) \left( \frac{1}{N} \sum_{i=1}^N \tilde{V}_{DC,i} - \tilde{V}_{DC,i} \right) \quad (32)$$

where  $K_{pBAL,i}$  is the voltage balancing proportional gain related to the  $i$ -th DC-link.  $T_{BAL,i}$  is the voltage balancing controller integral time constant, which is tuned to guarantee zero steady-state error.

Considering also the acquisition and the PWM time delay, the open loop transfer function of the voltage balancing control between the  $i$ -th DC-link voltage and  $\Delta\varphi_i$  can be easily derived by Fig. 8. It results in:

$$V_{DC,i}(s) = \frac{2G_\varphi}{3T_{DAB} C_i} \frac{1}{\left( s + \frac{1}{T_p} \right) \left( s + \frac{2}{3T_{DAB}} \right)} \left( \frac{s + \frac{1+G_V R_o}{R_o C_o}}{s + \frac{1}{R_o C_o}} \right) \Delta\varphi_i \quad (33)$$

Choosing  $T_{BAL,i} = T_p$  and thereby cancelling the slowest pole, the new open loop transfer function is:

$$G_{BAL,i}(s) \approx \frac{K_{pBAL,i} G_\varphi}{C_i s (1.5T_{DAB} s + 1)} \quad (34)$$

Eq. (34) shows the relationship between the parameters of the DC voltage balancing controller and the theoretical model of the ST.

For a comparison of the control schemes, the voltage balancing control performed by the CHB is shown in Fig. 9.

In Fig. 9  $V_{DC,i}$  is the DC voltage measured at the  $i$ -th DC-link of the CHB converter,  $i_g^*$  is the current reference and  $m_{BAL,i}$  represents the contribution to the modulating signal of the  $i$ -th H-Bridge in order to balance the DC voltage.

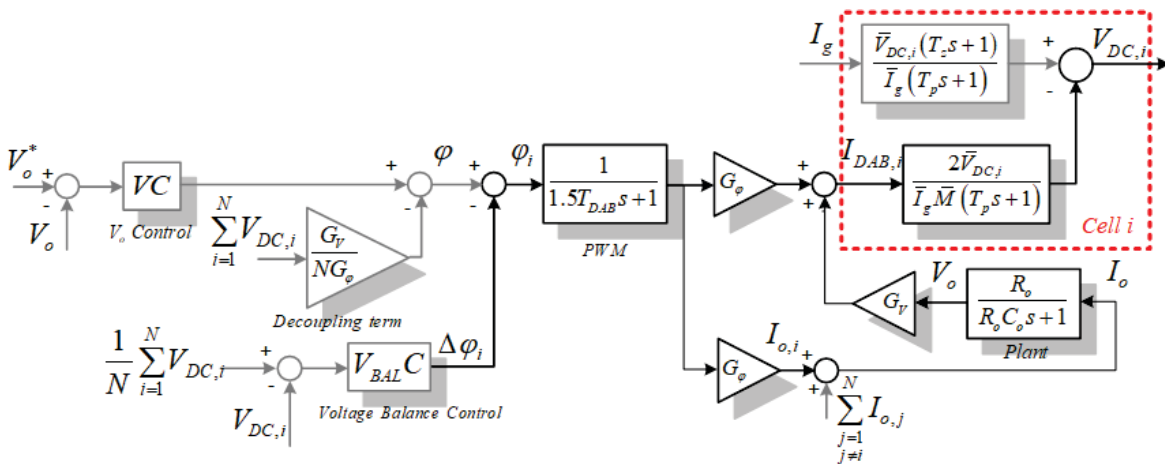


Fig. 8. Control scheme of the ST DC/DC power conversion stage.

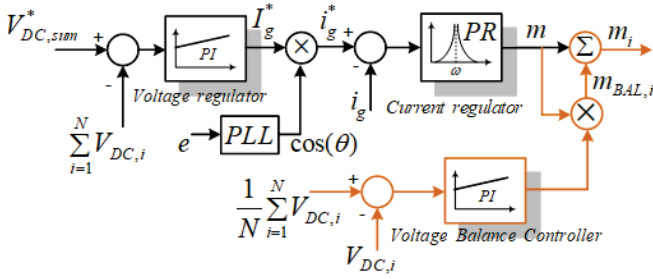


Fig. 9. CHB control scheme in case the CHB is balancing the voltages.

The modulating signal for the  $i$ -th H-Bridge is defined as:

$$m_i = m \left[ 1 + K_{pBAL, i} \left( 1 + \frac{1}{T_{BAL, i} s} \right) \left( \frac{1}{N} \sum_{i=1}^N V_{DC, i} - V_{DC, i} \right) \right] \quad (35)$$

where  $K_{pBAL, i}$  and  $T_{BAL, i}$  are respectively the proportional gain and the integral time constant of the  $i$ -th CHB cell voltage balancing controller. By varying the parameters, it is possible to regulate the control action.

The open loop transfer function of the voltage balancing loop  $G_{BAL, i}(s)$  can be derived by Fig. 10, where the PI controller transfer function, the model of the PWM time delay, the inductive grid filter and the  $i$ -th DC-link model are taken into account:

$$G_{BAL, i}(s) = \frac{M}{2} K_{pBAL, i} \left( 1 + \frac{1}{T_{BAL, i} s} \right) \left( \frac{1}{1.5T_s s + 1} \right) \left( \frac{1}{L_g s + R_g} \right) \left( \frac{R_i}{R_i C_i s + 1} \right) \quad (36)$$

#### IV. SIMULATION AND EXPERIMENTAL RESULTS

With the aim to validate the effectiveness of the proposed control structure and the theoretical models of the overall system, an experimental setup related to a small-scale ST has been built and it is shown in Fig. 11. Due to the experimental setup constraints, the first two stages of the ST consist of a 5-level CHB converter connected to the distribution grid and feeding power to two DAB converters. The DAB power modules are parallel connected in output and they supply a resistive load. The H-bridges in the CHB converter and the DAB converters are based on DP25H1200T101616IGBT Danfoss module and the system is controlled with a dSPACE SCALEXIO platform based on three DS2655FPGA boards; each board is programmed with a FPGA Xilinx blockset toolbox. The power stage parameters are summarized in Table I.

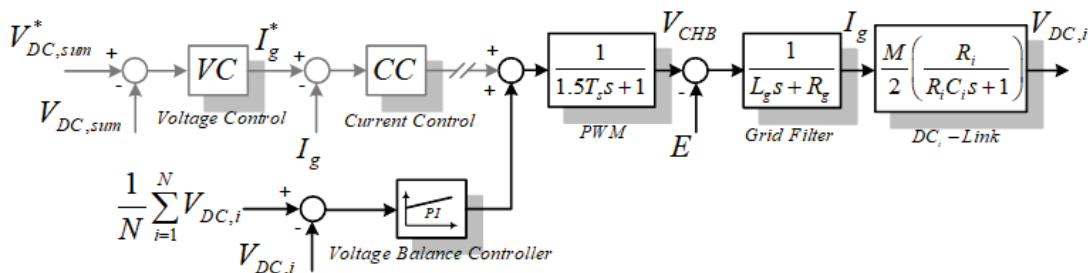


Fig. 10. Detailed voltage control scheme in case of voltage balancing in the CHB stage.

#### A. CHB and DAB converters model and control validation

For the validation of the CHB model, the responses of the system to a reference voltage step ( $\Delta V_{DC}^* = 10V$ ) are compared. This is shown in Fig. 12, where the step is applied at  $t=1s$  and the small signal model response, the average model response and experimental results are compared. As it can be seen, the voltage provided by the real system tracks the response provided by the models.

Similarly, the responses of the DAB converter in case of a reference voltage step ( $\Delta V_o^* = 1V$ ) have been compared by considering the output voltage provided experimentally and the results provided by the average and the small signal model in simulation. As in the previous case, the analytical results match well with the experimental results (Fig. 13). Finally, the effects of power variations on the DC-link voltages are analyzed: at  $t=0.5s$  the power processed by the first DAB converter is increased and the power processed by the second DAB converter is reduced by maintaining constant the overall output power. It can be observed that the power step implies a transient voltage variation for each DC-link and the small signal model response tracks the average model without significant deviations (Fig. 14).

#### B. Performance comparison of the balancing solutions

Finally, a comparison between the performances of the proposed voltage balancing technique and the voltage balancing performed by the CHB is provided. Considering the open loop transfer functions of the balancing loops, as reported in (34) for the DAB converters and in (36) for the CHB converter, the crossover frequency provides information about the bandwidth and the dynamics. For the DAB converters stage the bandwidth has been designed in order to obtain a voltage balancing control as fast as the current control loop in the CHB stage ( $f_{BW, CC} = 160 \text{ Hz}$ ). As a result, the phase margin is around  $75^\circ$ , which is a good compromise between robustness and dynamics.

For a fair comparison of the two balancing controllers, the bandwidth of the balancing control loop in the CHB stage has been chosen in order to guarantee the same robustness (same PM). The result in this case is a low bandwidth (4Hz). If the target is to reach a bandwidth of 160 Hz, the balancing method in the CHB stage is unstable. This demonstrates the better performance of the proposed balancing method in comparison to the classical approach.



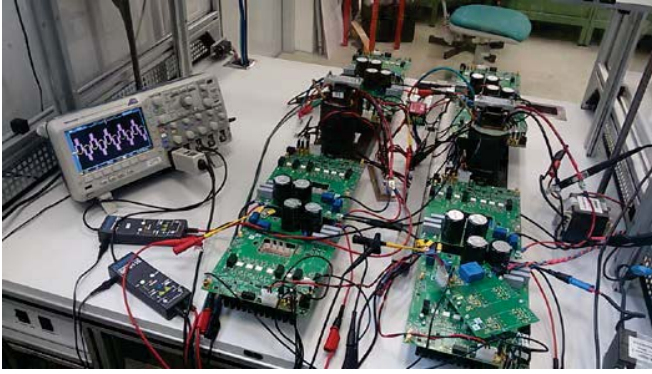


Fig. 11. Small-scale ST experimental setup: AC/DC and DC/DC power conversion stage.

TABLE I  
POWER STAGE PARAMETERS

Symbol	Description	Value
$e$	Grid Voltage (RMS)	230 V, 50 Hz
$L_g$	Filter Inductance (MV side)	3.8 mH
$V_{DC,1}=V_{DC,2}$	DC-Link voltage MV side	250 V
$V_o$	DC-link voltage LV side	250 V
$C_1=C_2$	MV capacitance	930 $\mu$ F
$C_o$	LV capacitance	920 $\mu$ F
$R_o$	Load resistance	32 $\Omega$
$L_{k,1}=L_{k,2}$	Leakage inductance MFT	63 $\mu$ H
$n$	MFT turn ratio	1
$f_{sw,CHB}$	CHB switching frequency	3 kHz
$f_{sw,DAB}$	DAB switching frequency	12 kHz
$P_n$	ST nominal power	2 kW

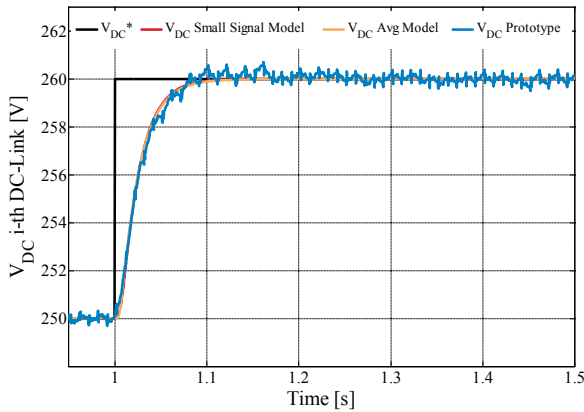


Fig. 12. CHB converter: response of the system in case of a reference voltage step  $\Delta V_{DC}^* = 10V$  ( $T_{setting} = 100ms$ ).

For the demonstration, the frequency responses of the two balancing controllers are shown in Fig. 15. A significant difference in the bandwidth ( $BW_{CHB} = 4Hz$ ,  $BW_{DAB} = 160Hz$ ) of the two control systems and consequently in the disturbance rejection capability is observed.

The voltage balancing control operated by the DC/DC power conversion stage of the ST exhibits superior performances than the voltage balance control operated by the AC/DC converter of the ST. This is because of the higher switching frequency in the DC/DC power conversion stage than in the CHB.

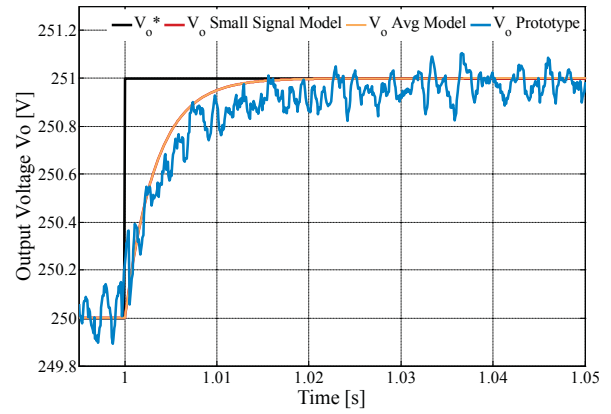


Fig. 13. DAB converters: response of the system in case of a reference voltage step  $\Delta V_o^* = 1V$  ( $T_{setting} = 10ms$ ).

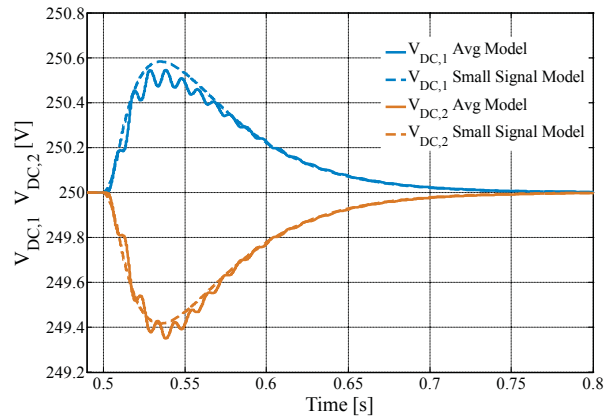


Fig. 14. DAB converters DC link voltages  $V_{DC,1}$  and  $V_{DC,2}$  in case of variations of the power processed by each cell.

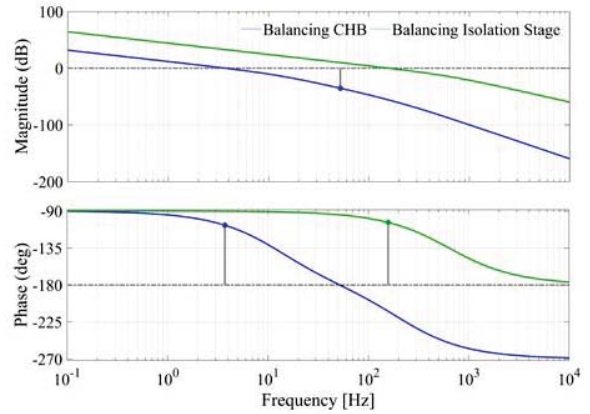


Fig. 15. Comparison of the bandwidth for voltage balancing in the CHB stage and in DAB converters stage.

The different dynamic performances can be observed also in Fig. 16 and Fig. 17 respectively, where the DC-link voltages of the 5 level CHB converter are shown moving from a power balance to a power unbalance condition. Starting from  $P_{DAB,1} = P_{DAB,2} = 1 kW$ , the DAB converters power reference are changed in  $P_{DAB,1} = 1,5 kW$  and  $P_{DAB,2} = 0,5 kW$ . As expected from Fig. 15, the response provided by the proposed control system is faster than the response of the voltage balancing performed by the CHB converter.

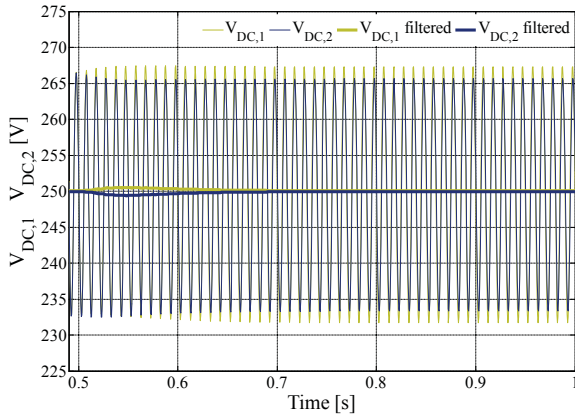


Fig. 16. DAB converters voltage balancing control: DC-link voltages in case of a power step for DAB<sub>1</sub> and DAB<sub>2</sub> (simulation results).

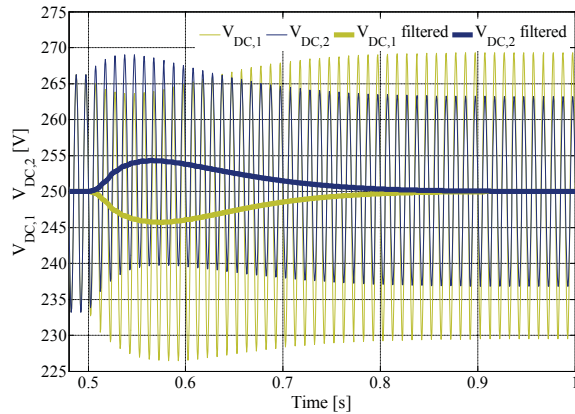


Fig. 17. CHB voltage balancing control: DC-link voltages in case of a power step for the two H-Bridges (simulation results).

The simulation results are validated experimentally with experiments similar to those performed previously. Results are shown in Fig. 18 and Fig. 19, respectively.

As expected from the simulation results, the transient behavior duration related to the balancing control in the DC/DC stage is shorter than the transient behavior duration related to the balancing control in the CHB stage and also the transient peak voltage is lower. It provides information about high rejection to external disturbances and it suggests using the voltage balancing method in the isolation stage rather than in the medium voltage stage. Remarkably, the experimental results fit the simulation results shown in Fig. 16 and Fig. 17.

Finally, Fig. 20 a) shows the output currents of the two DAB converters before and after the change in the power references. Before the change in the reference, the output currents of the DAB converters have the same mean value and their ripples are canceling out each other. The overall output current is  $I_o = 8A$ . After the power variation, the output currents of the DAB converters are respectively:  $I_{o,1} = 6A$  and  $I_{o,2} = 2A$ . Because of the unequal power sharing between the DAB converters, the currents exhibit higher harmonic distortion (Fig.20 b)). The increased distortion is the drawback of the presence of a circulating current path when the DAB converters work with different phase shift, sharing a different power to the load.

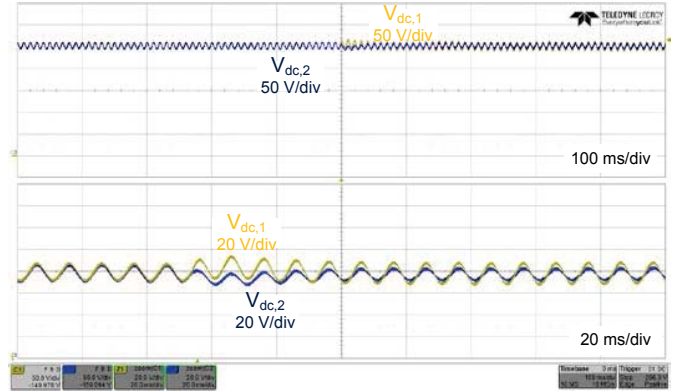


Fig. 18. DAB converters voltage balancing control: DC-link voltages in case of a power step for  $P_{DAB,1}$  and  $P_{DAB,2}$  (Experimental results)

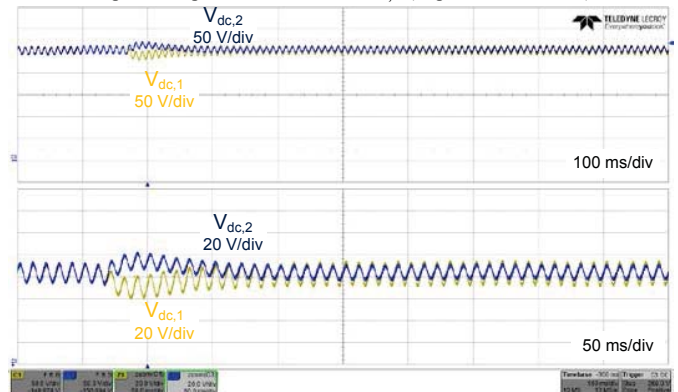


Fig. 19. CHB voltage balancing control: DC-link voltages in case of a power step for the two power modules (Experimental results).

## V. CONCLUSIONS

One of the main issues in a modular ST is the DC voltage balancing among the power cells. In case of a three-stage architecture based on a CHB converter for the AC/DC power conversion stage and DAB converters for the DC/DC power conversion stage, the CHB converter is commonly in charge of the voltage balancing. However, looking at the overall ST system, it can be advantageous that the DC/DC power conversion stage is in charge of the DC voltage balancing, because in DC Smart Grids the power flow is commonly not balanced. With the proposed control technique, the dynamic performance of the voltage balancing is improved, ensuring a larger bandwidth than the traditional control method. It is due to the higher switching frequency of the DC/DC power conversion stage than the switching frequency of the AC/DC power conversion stage.

## REFERENCES

- [1] G. J. Kish, "On the Emerging Class of Non-Isolated Modular Multilevel DC-DC Converters for DC and Hybrid AC-DC Systems," IEEE Transactions on Smart Grid, vol. PP, no. 99, pp. 1-1.
- [2] S. Grillo, V. Musolino, L. Piegari, E. Tironi and C. Tornelli, "DC Islands in AC Smart Grids," IEEE Transactions on Power Electronics, vol. 29, no. 1, Jan. 2014, pp. 89-98, 2014.
- [3] B. Wang, M. Sechilariu and F. Locment, "Intelligent DC Microgrid With Smart Grid Communications: Control Strategy Consideration and Design," IEEE Transactions on Smart Grid, vol. 3, no. 4, Dec. 2012, pp. 2148-2156, 2012.

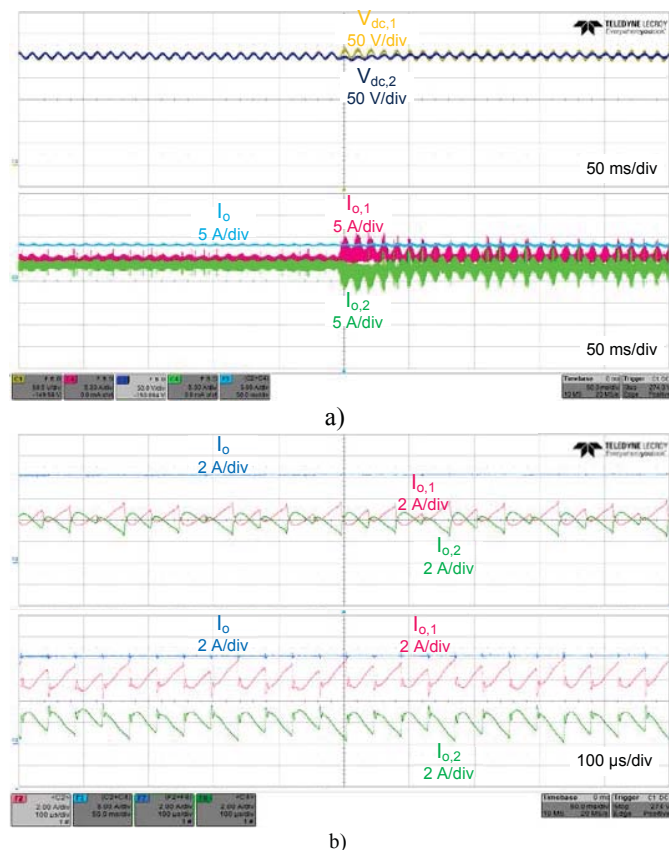


Fig. 20. DAB voltage balancing control: a) Output currents  $I_{o,1}$ ,  $I_{o,2}$ ,  $I_o$  during the variation; b) Zoom of the same currents.

[4] R. A. Mastromauro, S. Pugliese, D. Ricchiuto, S. Stasi and M. Liserre, "DC Multibus based on a Single-Star Bridge Cells Modular Multilevel Cascade Converter for DC smart grids," in Proc. 2015 International Conference on Clean Electrical Power (ICCEP), Taormina, Italy, pp. 55-60, 2015.  
 [5] Z. Jin, G. Sulligoi, R. Cuzner, L. Meng, J. C. Vasquez and J. M. Guerrero, "Next-Generation Shipboard DC Power System: Introduction Smart Grid and dc Microgrid Technologies into Maritime Electrical Networks", IEEE Electrification Magazine, vol. 4, no. 2, June 2016, pp. 45-57, 2016.  
 [6] F. D. Kanellos, G. J. Tsekouras and J. Prousalidis, "Onboard DC grid employing smart grid technology: challenges, state of the art and future prospects", IET Electrical Systems in Transportation, vol. 5, no. 1, pp. 1-11, 3 2015.  
 [7] T. Morstyn, B. Hredzak, G. D. Demetriades and V. G. Agelidis, "Unified Distributed Control for DC Microgrid Operating Modes", IEEE Transactions on Power Systems, vol. 31, no. 1, Jan. 2016, pp. 802-812, 2016.  
 [8] Z. X. Zou, G. De Carne, G. Buticchi and M. Liserre, "Smart Transformer-Fed Variable Frequency Distribution Grid," IEEE Transactions on Industrial Electronics, vol. 65, no. 1, Jan. 2018, pp. 749-759, 2018.  
 [9] X. Gao, F. Sossan, K. Christakou, M. Paolone and M. Liserre, "Concurrent Voltage Control and Dispatch of Active Distribution Networks by means of Smart Transformer and Storage," IEEE Transactions on Industrial Electronics, vol. 65, no. 8, Aug. 2018, pp. 6657-6666, 2018.  
 [10] T. L. Vandoorn, J. D. M. De Kooning, B. Meersman, J. M. Guerrero and L. Vandevelde, "Voltage-Based Control of a Smart Transformer in a Microgrid", IEEE Transactions on Industrial Electronics, vol. 60, no. 4, April 2013, pp. 1291-1305.  
 [11] R. Zhu, G. De Carne, F. Deng and M. Liserre, "Integration of Large Photovoltaic and Wind System by Means of Smart Transformer," in IEEE Transactions on Industrial Electronics, vol. 64, no. 11, Nov. 2017, pp. 8928-8938, 2017.  
 [12] H. Chen and D. Divan, "Design of a 10 kVA Soft-Switching Solid State Transformer (S4T)", IEEE Transactions on Power Electronics, vol. 33, no. 7, July 2018, pp. 5724-5738, 2018.

[13] B. Zhao, Q. Song, J. Li and W. Liu, "A Modular Multilevel DC-Link Front-to-Front DC Solid-State Transformer Based on High-Frequency Dual Active Phase Shift for HVDC Grid Integration", IEEE Transactions on Industrial Electronics, vol. 64, no. 11, Nov. 2017, pp. 8919-8927, 2017.  
 [14] M. Andresen, L. F. Costa, G. Buticchi and M. Liserre, "Smart Transformer reliability and efficiency through modularity", in Proc. 2016 IEEE 8th International Power Electronics and Motion Control Conference (IPEMC-ECCE Asia), Hefei, 2016, pp. 3241-3248.  
 [15] P. Xu et al., "The redundancy fault-tolerant control strategies for modular solid state transformer with DC bus", in Proc. 2017 IEEE 3rd International Future Energy Electronics Conference and ECCE Asia (IFEEC 2017 - ECCE Asia), Kaohsiung, 2017, pp. 1997-2001.  
 [16] L. F. Costa, G. Buticchi and M. Liserre, "Highly Efficient and Reliable SiC-Based DC-DC Converter for SmartTransformer", IEEE Transactions on Industrial Electronics, vol. 64, no. 10, Oct. 2017, pp. 8383-8392, 2017.  
 [17] T. Yao, I. Leonard, R. Ayyanar and M. Steurer, "Single-phase three-stage SST modeling using RTDS for controller hardware-in-the-loop application", in Proc. 2015 IEEE Energy Conversion Congress and Exposition (ECCE), Montreal, QC, 2015, pp. 2302-2309.  
 [18] L. F. Costa, G. Buticchi and M. Liserre, "Modular Smart Transformer architectures: An overview and proposal of an interphase architecture", in Proc. 2017 IEEE 8th International Symposium on Power Electronics for Distributed Generation Systems (PEDG), Florianopolis, 2017, pp. 1-7.  
 [19] D. Ricchiuto, R. A. Mastromauro, M. Liserre, I. Trintis and S. Munk-Nielsen, "Overview of multi-DC-bus solutions for DC microgrids", in Proc. 4th IEEE International Symposium on Power Electronics for Distributed Generation Systems (PEDG), Rogers, AR, 2013, pp. 1-8.  
 [20] L. Tarisciotti, P. Zanchetta, A. Watson, S. Bifaretti, J. C. Clare, and P. W. Wheeler, "Active dc voltage balancing PWM technique for high power cascaded multilevel converters", IEEE Transactions on Industrial Electronics, vol. 61, no. 11, Nov. 2014, pp. 6157-6167, 2014.  
 [21] M. Moosavi, G. Farivar, H. Iman-Eini and S. M. Shekarabi, "A voltage balancing strategy with extended operating region for cascaded H-bridge converters", IEEE Transactions on Power Electronics, vol. 29, no. 9, Sept. 2014, pp. 5044-5053.  
 [22] A. Moeini and S. Wang, "A DC Link Voltage Balancing Technique for Cascaded H-Bridge Multilevel Converters with Asymmetric Selective Harmonic Current Mitigation-PWM", IEEE Transactions on Power Electronics, vol. PP, no. 99, pp. 1-1.  
 [23] J. A. Barrena, L. Marroyo, M. Á. Rodríguez Vidal and J. R. Torrealday Apraiz, "Individual Voltage Balancing Strategy for PWM Cascaded H-Bridge Converter-Based STATCOM", IEEE Transactions on Industrial Electronics, vol. 55, no. 1, Jan. 2008, pp. 21-29, 2008.  
 [24] H. Iman-Eini, J. L. Schanen, S. Farhangi and J. Roudet, "A Modular Strategy for Control and Voltage Balancing of Cascaded H-Bridge Rectifiers", IEEE Transactions on Power Electronics, vol. 23, no. 5, Sept. 2008, pp. 2428-2442, 2008.  
 [25] J. I. Leon, R. Portillo, S. Vazquez, J. J. Padilla, L. G. Franquelo and J. M. Carrasco, "Simple Unified Approach to Develop a Time-Domain Modulation Strategy for Single-Phase Multilevel Converters", IEEE Transactions on Industrial Electronics, vol. 55, no. 9, Sept. 2008, pp. 3239-3248, 2008.  
 [26] X. She, A. Q. Huang, T. Zhao and G. Wang, "Coupling Effect Reduction of a Voltage-Balancing Controller in Single-Phase Cascaded Multilevel Converters", IEEE Transactions on Power Electronics, vol. 27, no. 8, Aug. 2012, pp. 3530-3543, 2012.  
 [27] T. Zhao, G. Wang, S. Bhattacharya, and A. Q. Huang, "Voltage and power balance control for a cascaded h-bridge converter-based solid state transformer," IEEE Transactions on Power Electronics, vol. 28, no. 4, April 2013, pp. 1523-1532, 2013.  
 [28] X. Wang, J. Liu, S. Ouyang, T. Xu, F. Meng and S. Song, "Control and Experiment of an H-Bridge-Based Three-Phase Three-Stage Modular Power Electronic Transformer", IEEE Transactions on Power Electronics, vol. 31, no. 3, March 2016, pp. 2002-2011.  
 [29] V. Raveendran, G. Buticchi, A. Mercante and M. Liserre, "Comparison of voltage control methods of CHB converters for power routing in smart transformer", in Proc. 2017 IEEE Energy Conversion Congress and Exposition (ECCE), Cincinnati, OH, USA, 2017, pp. 1652-1658.  
 [30] J. Shi, W. Gou, H. Yuan, T. Zhao and A. Q. Huang, "Research on voltage and power balance control for cascaded modular solid-state transformer", IEEE Transactions on Power Electronics, vol. 26, no. 4, April 2011, pp. 1154-1166, 2011.  
 [31] K. Xu, C. Fu, Y. Wang and H. Wang, "Voltage and current balance control for the ISOP converter-based power electronic transformer", in Proc.

18th International Conference on Electrical Machines and Systems (ICEMS), Pattaya, 2015, pp. 378-382.

[32] M. Andresen, V. Raveendran, G. Buticchi and M. Liserre, "Lifetime-based Power Routing in Parallel Converters for Smart Transformer Application", *IEEE Transactions on Industrial Electronics*, vol. 65, no. 2, Feb. 2018., pp. 1675-1684.

[33] V. Raveendran, M. Andresen, M. Liserre and G. Buticchi, "Lifetime-based power routing of smart transformer with CHB and DAB converters", in *Proc. 2018 IEEE Applied Power Electronics Conference and Exposition (APEC)*, San Antonio, TX, 2018, pp. 3523-3529.

[34] Z. Zhang, H. Zhao, S. Fu, J. Shi and X. He, "Voltage and power balance control strategy for three-phase modular cascaded solid stator transformer", in *Proc. 2016 IEEE Applied Power Electronics Conference and Exposition (APEC)*, Long Beach, CA, 2016, pp. 1475-1480.

[35] H.-J. Yun, H.-S. Kim, M.-H. Ryu, J.-W. Baek, and H.-J. Kim, "A simple and practical voltage balance method for a solid-state transformer using cascaded h-bridge converters", in *Proc. IEEE 2015 9th International Conference on Power Electronics and ECCE Asia (ICPE-ECCE Asia)*, 2015, pp. 2415-2420.

[36] Y. Liu, A. Q. Huang, W. Song, S. Bhattacharya and G. Tan, "Small-Signal Model-Based Control Strategy for Balancing Individual DC Capacitor Voltages in Cascade Multilevel Inverter-Based STATCOM", *IEEE Transactions on Industrial Electronics*, vol. 56, no. 6, June 2009, pp. 2259-2269, 2009.

[37] M. Khazraei, V. A. K. Prabhala, R. Ahmadi and M. Ferdowsi, "Solid-state transformer stability and control considerations", in *Proc. 2014 IEEE Applied Power Electronics Conference and Exposition - APEC 2014*, Fort Worth, TX, 2014, pp. 2237-2244.

[38] H. Sun, J. Zhang and C. Fu, "Control strategy for dual active bridge based DC solid state transformer", in *Proc. 20th International Conference on Electrical Machines and Systems (ICEMS)*, Sydney, NSW, 2017, pp. 1-6.

[39] J. A. Mueller and J. W. Kimball, "Generalized average modeling of DC subsystem in solid state transformers", in *Proc. 2017 IEEE Energy Conversion Congress and Exposition (ECCE)*, Cincinnati, OH, 2017, pp. 1659-1666.

[40] J. E. Huber, J. W. Kolar, "Optimum number of cascaded cells for high-power medium-voltage AC-DC converters", *IEEE Journal of Emerging and Selected Topics in Power Electronics*, vol. 5, no. 1, March 2017, 2017.

[41] A. Rodríguez Alonso, J. Sebastian, D. G. Lamar, M. M. Hernandez and A. Vazquez, "An overall study of a Dual Active Bridge for bidirectional DC/DC conversion", in *Proc. 2010 IEEE Energy Conversion Congress and Exposition*, Atlanta, GA, 2010, pp. 1129-1135.

[42] R. A. Mastromauro, M. Liserre and A. Dell'Aquila, "Study of the Effects of Inductor Nonlinear Behavior on the Performance of Current Controllers for Single-Phase PV Grid Converters", *IEEE Transactions on Industrial Electronics*, vol. 55, no. 5, May 2008, pp. 2043-2052, 2008.

[43] R. Teodorescu, M. Liserre, P. Rodriguez, "Grid Converters for photovoltaic and Wind Power Systems", John Wiley and Sons Ltd., 2011.



**Sante Pugliese** received the M.Sc. degree in automation engineering in 2013 and the Ph.D. degree in electrical and information engineering in 2018 from the Politecnico di Bari, Italy. In 2017 he was a visiting scholar at the Chair of Power Electronics of Kiel, Germany, where actually he is a post-doctoral researcher. His research interests include power converters and control techniques for distributed power generation systems based on renewable energies.



**Markus Andresen** (S'15-M'17) received the M.Sc. degree in electrical engineering and business administration in 2012 and the Ph.D. degree in 2017 from the chair of power electronics at Christian-Albrechts-University of Kiel, Germany. In 2010, he was an intern in the Delta Shanghai Design Center at Delta Electronics (Shanghai) Co., Ltd., China and in 2017 he was a visiting scholar at the University of Wisconsin-Madison, USA. His current research interests include control of power converters and reliability in power electronics.



**Rosa A. Mastromauro** (S'05 - M'10) received the M.Sc. and Ph.D. degrees in electrical engineering from the Politecnico di Bari, Bari, Italy, in 2005 and 2009, respectively. Since 2005, she has been with the Power Converters, Electrical Machines, and Drives Research Team, Politecnico di Bari, where she was an Assistant Professor. Currently she is an Associate Professor at the University of Florence, Florence, Italy, and she is engaged in teaching courses in power electronics and electrical machines. Her research interests include power converters and control techniques for distributed power generation systems, renewable energies and transportation applications. Prof. Mastromauro is a member of the IEEE Industrial Electronics Society, IEEE Power Electronics society, IEEE Industrial Application Society, IEEE Women in Engineering Society. She is Associate Editor of the *IEEE Transactions on Industrial Electronics*. She is a reviewer for IEEE conference proceedings and journals.



**Giampaolo Buticchi** (S'10-M'13-SM'17) received the Masters degree in Electronic Engineering in 2009 and the Ph.D. degree in Information Technologies in 2013 from the University of Parma, Italy. In 2012 he was visiting researcher at The University of Nottingham, UK. Between 2014 and 2017 he was a post-doctoral researcher at the University of Kiel, Germany. He is now Associate Professor in Electrical Engineering at The University of Nottingham Ningbo China. His research area is focused on power electronics for renewable energy systems, smart transformer fed micro-grids and dc grids for the More Electric Aircraft. He is author/co-author of more than 140 peer-reviewed scientific papers. He is an Associate Editor of the *IEEE Transactions on Industrial Electronics*.



**Silvio Stasi** was born in Bari, Italy, in 1958. He received the MSc degree in Electrical Engineering from the University of Bari, Italy, and the PhD degree in Electrical Engineering from Politecnico di Bari, in 1993. From 1990 to 1993, he was with the Electric Drives and Machines Group, Politecnico di Bari, where he carried out research on control and state and parameter estimation of electrical drives and, since November 2002, has been an Associate Professor of electrical machines and drives in the Department of Electrical and Information Engineering. His research interests include control of electric drives, fuzzy logic, neural networks, power electronics, motor parameter estimation.



**Marco Liserre** (S'00-M'02-SM'07-F'13) received the MSc and PhD degree in Electrical Engineering from the Bari Polytechnic, respectively in 1998 and 2002. He has been Associate Professor at Bari Polytechnic and Professor in reliable power electronics at Aalborg University (Denmark). He is currently Full Professor and he holds the Chair of Power Electronics at Christian-Albrechts-University of Kiel (Germany). He has published over 300 technical papers (more than 100 of them in international peer-reviewed journals), 4 chapters of a book and a book (Grid Converters for Photovoltaic and Wind Power

Systems, ISBN-10: 0-470-05751-3-IEEE-Wiley, second reprint, also translated in Chinese). These works have received more than 20000 citations. Marco Liserre is listed in ISI Thomson report "The world's most influential scientific minds" from 2014. He has been awarded with an ERC Consolidator Grant for the project "The Highly Efficient And Reliable smart Transformer (HEART), a new Heart for the Electric Distribution System". He is member of IAS, PELS, PES and IES. He is Associate Editor of the IEEE Transactions on Industrial Electronics, IEEE Industrial Electronics Magazine, IEEE Transactions on Industrial Informatics, where he is currently Co-Eic, IEEE Transactions on power electronics and IEEE Journal of Emerging and Selected Topics in Power Electronics. He has been Founder and Editor-in-Chief of the IEEE Industrial Electronics Magazine, Founder and the Chairman of the Technical Committee on Renewable Energy Systems, Co-Chairman of the International Symposium on Industrial Electronics (ISIE 2010), IES Vice-President responsible of the publications. He has received the IES 2009 Early Career Award, the IES 2011 Anthony J. Hornfeck Service Award, the 2014 Dr. Bimal Bose Energy Systems Award, the 2011 Industrial Electronics Magazine best paper award and the Third Prize paper award by the Industrial Power Converter Committee at ECCE 2012, 2012. He is senior member of IES AdCom. In 2013 he has been elevated to the IEEE fellow grade with the following citation "for contributions to grid connection of renewable energy systems and industrial drives".